NASA Technical Memorandum 79250

MARANGONI BUBBLE MOTION IN ZERO GRAVITY

Robert L. Thompson
Lewis Research Center
Cleveland, Ohio

and

Kenneth J. De Witt
The University of Toledo
Toledo, Ohio

Prepared for the
Seventy-second Annual Meeting of the American Institute of Chemical Engineers
San Francisco, California, November 25-29, 1979

MARANGONI BUBBLE MOTION IN ZERO GRAVITY

by Robert L. Thompson
National Aeronautics and Space Administration
Lewis Research Center
Cleveland, Ohio 44135

and

Kenneth J. De Witt
The University of Toledo
Toledo, Ohio 43606

E-160

ABSTRACT

For the first time, it has been shown experimentally that the Marangoni phenomenon is a primary mechanism for the movement of a gas bubble in a non-isothermal liquid in a low-gravity environment. In such a two-phase flow system, local variations in surface tension at the bubble surface are caused by a temperature gradient in the liquid. Shearing stresses thus generated at the bubble surface lead to convection in both media, as a result of which the bubble begins to move. A mathematical model consisting of the Navier-Stokes and thermal energy equations, together with the appropriate boundary conditions for both media, is presented. Parameter perturbation theory is used to solve this boundary value problem; the expansion parameter is the Marangoni number. The zeroth, first- and second-order approximations for the velocity, temperature and pressure distributions in the liquid and in the bubble, and the deformation and terminal velocity of the bubble are determined. Experimental zero-gravity data for a nitrogen bubble in ethylene glycol, ethanol, and silicone oil subjected to a linear temperature gradient were obtained using the NASA Lewis zero-gravity drop tower. Comparison of the zeroth order analytical results for the bubble terminal velocity showed good agreement with the experimental measurements. The first- and second-order solutions for the bubble

deformation and bubble terminal velocity are valid for liquids having Prandtl numbers on the order of one, but there is a lack of appropriate data to test the theory fully.

INTRODUCTION

The Marangoni flow phenomenon, the flow generated by a gradient in surface tension, could be the driving flow mechanism in a low-gravity environment. Because of the role of this flow phenomenon in materials processing in space, fluid storage and transfer operations in space, and boiling heat transfer as applied to propellant management in space, it is receiving increasing study.

The phenomenon of surface tension induced flow requires a liquid-vapor interface and local variations in interfacial tension. In this two-phase flow system, local variations in the surface tension at the bubble interface are caused by temperature variations in the liquid and gaseous media. According to the Marangoni flow phenomenon, liquid should flow around the bubble and the bubble should migrate toward the hotter region. However, it is difficult to study this flow phenomenon in normal gravity because of buoyancy effects. In normal gravity, buoyancy driven flows generally mask surface tension induced flows, that is, the magnitude of the buoyancy force is much greater than the thermophoretic force and buoyancy driven convection may further complicate the study. It is, therefore, virtually impossible to carry out a quantitative experimental investigation for "pure" surface tension induced flows in normal gravity. As a result, the experimental investigation of this flow phenomenon was conducted in the NASA Lewis Research Center Zero-Gravity Facility.

The primary objective of this work was to observe the behavior of a single noncondensible bubble in a liquid under the influence of a linear temperature gradient in a weightless environment, and then to compare these experimental

data with existing theory. A secondary objective was to extend the analytical model of this flow phenomenon beyond that which is presently available.

Although the Marangoni flow phenomenon is a classical fluid physics problem, only a limited amount of experimental and analytical work has been done in this area for the reasons mentioned above. Hershey in 1939 (ref. 1) conducted an experiment in which it was shown that if a temperature gradient exists along a free liquid-vapor interface, a dynamic steady state is achieved. Block in 1956 (ref. 2) carried out experiments to prove that Benard (convection) cell motions are produced by variations in the surface tension due to thermal gradients. The first experimental work concerned with the study of surface tension induced flow of a bubble in a heated liquid was done by Young, Goldstein, and Block in 1959 (ref. 3). Experimentally, they obtained a temperature gradient in a liquid sufficient to hold a bubble stationary in normal gravity by balancing the gravity force with the thermophoretic force. Their experimental data was in fair agreement with their theoretical predictions. Hardy (ref. 4) repeated Young, et al.'s experiment in a more precise manner, and concluded that his data were in good agreement with the previous study. McGrew in 1968 (ref. 5) conducted experiments to verify the theory he developed for computing the static thermophoretic force on a bubble. Papazian and Wilcox (ref. 6) were the first to conduct a Marangoni experiment in a low-gravity environment. Using a Space Processing Applications Research (SPAR) sounding rocket to achieve this type of environment, they were not successful in observing this flow phenomenon, primarily due to experimental difficulties. Theoretical analyses similar to that of Young, et al., were performed by Kuznetsov, et al. (ref. 7) and by Lyubin and Povitskiy (ref. 8). Bratukhin's analysis (ref. 9) differed from the previous investigators in that perturbation theory was used, where the dependent variables were expressed in a series expansion with the Marangoni number being the control parameter.

To date, relatively few quantitative experimental measurements of the Marangoni bubble motion flow phenomenon have been made to compare with the theory. The theory developed by the above investigators has been limited to the solution of the linearized Navier-Stokes equations (creeping flow approximation) and the assumption of pure conduction which permitted the use of Laplace's equation, together with the appropriate boundary conditions on velocity, stress, and temperature. For a spherical bubble, the corrected expression for the bubble terminal velocity as determined by Young, et al. is

$$U = \frac{2}{3}\frac{1}{\mu_1}\frac{1}{(2\mu_1 + 3\mu_2)}\left[\frac{3\mu_1 a}{2 + h_2/h_1}\frac{d\sigma}{dT}\frac{dT}{dz} - (\rho_1 - \rho_2)ga^2(\mu_1 + \mu_2)\right] \qquad (1)$$

(See the symbol list for definitions of the quantities.) By setting the velocity equal to zero and neglecting the ratios of viscosities, densities, and thermal conductivities of the inner to outer media, the temperature gradient required to hold the bubble motionless can be found and is given by

$$\frac{dT}{dz} = \frac{2\rho_1 ga}{3\, d\sigma/dT} \qquad (2)$$

EXPERIMENTAL PROGRAM

Initially, there were three key feasibility issues identified. The first had to do with the development of a bubble injection system to introduce a single bubble into the liquid with minimal disturbance to the liquid and such that bubble size could be controlled. The second had to do with the development of a heating system to establish and maintain a linear temperature gradient in the liquid without causing any buoyancy driven convection. The third issue was an operational one, that is, the test run had to be completed within an 8-hour time shift. Other concerns were the selection of test liquids, the determination of tank size, safety considerations, effect of bubble oscillations, selection of temperature instrumentation, visual observation of bubble behavior, effect of surface contamination, drop-tower limitations, etc.

Based on the above mentioned key feasibility issues and other concerns, the experimental apparatus used to observe the Marangoni flow phenomenon was designed around the Lewis Research Center's 155 m zero-gravity facility, shown in Figure 1. Data were obtained by allowing a capsule housing the experiment to free-fall for a time of 5.2 seconds.

Experimental Apparatus

A schematic of the experimental apparatus is shown in Figure 2. A cylindrical test container, 12 cm in diameter and 12 cm high was fabricated from a transparent plastic material to permit visual observation of the bubble rising in the liquid. The container side walls were insulated using a vacuum jacket fabricated from a transparent plastic material. The bubble injection system consisted of a supply of pressurized gas, a valving system consisting of a micrometer valve and a solenoid valve mounted in series, and a nozzle. A noncondensible bubble (nitrogen) was formed and introduced into the liquid from a submerged orifice at the bottom of the test compartment. To establish and maintain the desired temperature gradient, a heater was employed at the top of the test container and a cooling bath at the bottom. Thermocouples attached to a rake, 2 cm apart and 3 cm from the tank centerline, were employed to monitor the liquid temperature before and during the test drop. Another thermocouple embedded in the heater plate was employed to monitor the plate temperature. The bubble movement was recorded by two high-speed cameras which were mounted 90° apart to observe the motion if the bubble path deviated from rectilinear. The elapsed free-fall time was obtained from two digital clocks in view of the cameras. A centimeter scale was mounted to the lower plate for scaling purposes. The bubble distortion resulting from the refractive index of the cylindrical tanks was accounted for when the data were analyzed. A photograph of the test apparatus is shown in Figure 3.

Initial Tests - Feasibility Issues

Preliminary zero-gravity tests were conducted to verify the bubble injection system. The bubble was introduced into the liquid a fraction of a second after the drop was initiated. As a result of these tests, several experimental problems of Marangoni flow became apparent. First, a finite time for bubble oscillations to damp out was required, leaving fewer seconds of free-fall time to observe the Marangoni flow phenomenon. Second, the bubble had an apparent residual velocity even after 5.2 seconds of free-fall time. To illustrate these problems, Figure 4 shows a representative plot of bubble displacement as a function of free-fall time for distilled water. The bubble residual velocity still persists after 5.2 seconds of free-fall time, but it appears to be decaying roughly exponentially. Also, note on the figure the free-fall time at which the bubble oscillations damped out as determined photographically. In other tests, methylene blue dye was introduced into the liquid to determine liquid disturbance as a result of bubble injection. These tests showed that the initial disturbance to the liquid decayed rapidly, and no gross motion of the liquid occurred. It was noted, however, that the dye affected the bubble formation and separation processes, and it was impossible to form a single bubble.

Besides the bubble injection system, another key feasibility issue identified at the onset of this experin ent was whether or not the desired temperature gradient could be established and maintained in the liquid. The apparatus just described was designed with the intent of having the greatest flexibility for realizing this objective, without having any buoyancy driven convection present. Preliminary ground tests were conducted with distilled water to see if a linear temperature gradient could be obtained, and to determine the required heating time. Figure 5 shows a representative temperature profile after 260 minutes of heating. As can be seen, a linear temperature gradient is approached in the top half of the tank. The liquid was heated from the top to avoid Raleigh insta-

bilities. Radial heat loss was minimized by the sidewall vacuum jacket insulation. As a further check to insure there was no buoyancy driven convection present, a separate thermocouple probe was used to measure the liquid temperature along the centerline axis of the container. As the thermocouple was lowered into the liquid through the standpipe, it took only a few seconds for the measurements to stabilize at each position. The results, when compared with the temperatures measured 3 cm from the centerline, were nearly identical, indicating there was no buoyancy driven convection occurring within an annulus of fluid approximately 6 cm in diameter.

Another key feasibility issue identified early in the program was the time required for a test. Although it was an operations problem rather than a technical one, it was imperative that a test be completed with an 8-hour working shift. Time estimates of the various phases of the test program included ground preparation, transport of the experiment vehicle, heating of the liquid, evacuating of the drop chamber, and recovery of the experiment. Summing up the maximum time estimates for each of the test stages, it was found that a complete test could be completed within an 8-hour time frame.

Test Fluids

Several factors were taken into consideration in the selection of the test fluids, the most important being the thermophysical properties, clarity, presence of surfactants, and potential safety and health problems. The liquids chosen were distilled water, ethylene glycol, DC 200 silicone oil, and ethanol. Although distilled water is known to contain surfactants, it was chosen because of its high surface tension gradient and safety considerations, and was expected to provide experimental data outside the creeping flow regions. Ethylene glycol and silicone oil were selected because any surface active agents present tend to stay in the bulk phase rather than migrate to the bubble surface. Ethanol was chosen because it is available as a reagent grade pure liquid, and experimental

data can be obtained outside the creeping flow regime. A table of properties of these four test liquids is shown in Table 1.

EXPERIMENTAL RESULTS

Meaningful data were obtained from about 80 percent of the 38 tests performed in the 155 m drop tower. Complete results are presented by the author in reference 10. Single bubbles were generated in about half of the tests, but the tests when multiple bubbles were formed (generally two) were also of value and arguments are presented to validate their usefulness. The importance of the nozzle configuration is also discussed, as are bubble displacements, bubble size, shape, and oscillation measurements. The nozzle characteristics which were varied in the experiment included the nozzle height, that is, the distance measured from the bottom of the test container to the top of the nozzle, the inside diameter, and the nozzle material.

The basic raw data collected from the experiments consisted of (1) taking bubble displacement measurements as a function of free-fall time from the films; (2) bubble shape measurements as a function of time; and (3) bubble oscillations as a function of time. For accuracy of measurement and convenience, bubble displacement was measured from the orifice to the bottom of the bubble, while the time was measured from the initiation of free-fall. Bubble shapes were corrected for distortion using appropriate scale factors, while the bubble oscillations, after the initial vertical rise, were in the second mode, that is, the bubble oscillates between an oblate and prolate shape.

Figure 6 shows the comparison of a typical isothermal run with a typical nonisothermal run for distilled water. As can be seen, the isothermal bubble displacement was continually decreasing with time, having a residual velocity of 0.3 cm/sec in the last second of free-fall. The nonosithermal run shown is the one having the greatest displacement as a function of time with a bubble terminal velocity of 0.6 cm/sec in the last second of free-fall when the tem-

perature gradient was about 4° C/cm. Since the expected value of velocity is an order of magnitude greater than this, there is very little discernible difference between the velocities obtained from these curves, and it appears that the Marangoni flow phenomenon was not observable using distilled water. In addition, it should be noted that a single bubble was not generated in any of these runs. Marangoni flow was not observed in distilled water. This may have been because of surfactants concentrated at the bubble surface or because of some molecular phenomenon, perhaps caused by the polar nature of the water molecule, that occurred at the bubble interface. Either of these factors could eliminate or change the surface tension gradient.

For the other three test liquids, ethylene glycol, DC 200 silicone oil, and ethanol, Marangoni flow was observed. Figure 7 is representative of the experimental data obtained for the three test liquids. In this figure, data are presented for ethylene glycol. Bubble displacement is plotted as a function of free-fall time for four temperature gradients ranging from 1.0° to 4.0° C/cm. For comparative purposes, results for an isothermal run are also shown. The results show that the bubble displacement for the nonisothermal cases becomes nearly linear with time, indicating that the bubble reached a terminal velocity. The bubble displacement for the isothermal case becomes relatively flat, having a residual velocity of less than 0.05 cm/sec over the last second of free-fall time. Bubble diameter for each of these test runs was approximately 0.8 cm. The bubble shape, after the oscillations damped out in less than 0.2 seconds, was spherical. Some of the test data when multiple bubbles were formed was used. Although the bubbles are following mutually perpendicular paths, arguments supported by experimental data indicate the usefulness of the data depending on the relative sizes of the bubbles and their separation distance, as shown by the author (ref. 10). Some of the more important multiple-bubble data results are now breifly discussed.

In this study, the principle interest was in observing the classical-fluid physics Marangoni flow phenomenon for a single bubble in a zero-gravity environment. The experimental bubble terminal velocity and bubble shape data were to be compared with existing theory, and an extension to the theory developed as part of this dissertation. However, in the actual case of materials processing in space, multiple bubbles will likely be present. Consequently, future investigations of the Marangoni bubble phenomenon should include studies of multiple bubble interaction effects as well as a continuation of single bubble experimentation. As determined from the experimental data, important multiple bubble interaction factors include: the relative bubble sizes, whether a bubble is leading or trailing another bubble, bubble separation distance, and relative bubble paths, that is, whether the paths are perpendicular, parallel, or at some other angle. Some of the conclusions reached from the limited amount of experimental data obtained indicate that bubble interaction effects is a very worthwhile area to pursue. For example, for two bubbles, it was determined that the leading bubble wake does affect the temperature distribution field around the trailing bubble, especially when the paths are perpendicular. In this case, if the leading bubble is the larger one, its terminal velocity does not appear to be affected, whereas the trailing bubble velocity is greatly affected and, in some cases, the trailing bubble comes to rest. On the other hand, when the trailing bubble is the larger one, it rises faster, indicating the wake effect of the leading bubble is minimal on the trailing bubble, and the bubbles should coalesce. In the cases where the bubble paths were not perpendicular, there appeared to be little bubble interaction effects even when the leading bubble was larger than the trailing bubble. Of course, the bubble sizes as well as bubble separation distance also affect the bubble terminal velocities.

In addition to the bubble-bubble interaction phenomenon, another interesting phenomenon which was observed in practically all the isothermal zero-

gravity tests was that, regardless of the test liquid used, the bubbles after 5.0 seconds of zero-gravity time still had some residual velocity. Longer zero-gravity times are required to determine how long it would take for the bubble to approach zero velocity since the only force acting on the bubble interface is the drag force. The conclusion reached from the experimental results is that the residual velocity, after 5.0 seconds of free-fall time, is inversely dependent on the viscosity of the liquid. For all test liquids used, the bubble velocity decay rate appears to be exponential.

Also, it was observed that the bubble size did not change during the 5.0 seconds of free-fall time, which indicates that there was no observable bubble expansion during this time due to the heating of the bubble. To study the heating effect on bubble expansion would require much longer zero-gravity times than can be obtained in a ground-based research facility and, therefore, this would have to be conducted in a space environment.

Some representative data for the three test liquids are shown in Figure 8. The linear temperature gradient for the silicone oil was on the order of 2^{o} C/cm, whereas for ethylene glycol and ethanol, it was on the order of 4^{o} C/cm. The circles represent the relative bubble sizes, which for silicone oil and ethylene glycol were on the order of 0.8 cm, while for ethanol the size was approximately 0.6 cm. A teflon tip nozzle was used for the ethanol as opposed to a stainless steel tip nozzle for the other two fluids. Note from the figure the nearly linear displacement as a function of time for all three liquids, indicating in each case that the bubble reached terminal velocity.

As an illustration of the role of the nozzle configuration in the formation of a single bubble, the following discussion is presented for ethylene glycol as the test fluid. Initially, a nozzle height of 9 cm was chosen, but multiple bubbles were always formed by a stainless steel nozzle. In addition, it was

observed that the proximity of the top plate affected the bubble displacement. As a consequence of having these undesirable conditions, a nozzle height of 6 cm was chosen, which again resulted in multiple bubbles. A teflon tip was placed over the stainless steel nozzle with the same diameter in an effort to form a single bubble. This solution was partially successful in that a single bubble was formed, but not until late into the drop. The late bubble formation was attributed to the relative difference in the contact angle between the teflon and the stainless steel. A final attempt to produce a single bubble was made using a smaller diameter orifice. Decreasing the orifice inside diameter from 0.066 to 0.043 cm and a height of 6 cm enabled three single bubble experiments to be conducted.

The experimental data obtained in this study are correlated in terms of two dimensionless parameters, the Reynolds number and the Marangoni number. The Reynolds number, a ratio of inertial to viscous forces, is given by

$$\mathrm{Re} = \frac{\rho_1 a U}{\mu_1} \tag{3}$$

and the Marangoni number is given by

$$\mathrm{Ma} = \frac{\Delta\sigma}{\Delta T}\frac{\Delta T}{\Delta z}\frac{\rho_1 a^2}{\mu_1^2} \tag{4}$$

where U = bubble terminal velocity, a = bubble radius, μ_1 = liquid viscosity, ρ_1 = liquid density, $\Delta\sigma/\Delta T$ = surface tension gradient, and $\Delta T/\Delta z$ = temperature gradient.

ANALYSIS

In developing the mathematical analysis for the problem, the following assumptions are made. The problem is formulated as being steady state with uniform streaming flow and a linear temperature gradient at infinity. Axial symmetry exists in spherical coordinates and the bubble is allowed to deviate

slightly from spherical. The two media, gas and liquid, are assumed to be immiscible, and the liquid is Newtonian. The force of gravity is neglected and the thermophysical properties of the two media are constant, that is, density, specific heat, thermal conductivity, and viscosity, even though the temperature is varying. The one quantity allowed to vary is the surface tension σ, which, for most liquids, depends linearly on temperature. Mathematically, the surface tension variation can be expressed as

$$\sigma = \overline{\sigma}_o + \frac{d\sigma}{dT} \Delta T \tag{5}$$

where σ_o is a reference surface tension at temperature T_o and the surface tension gradient, $d\sigma/dT$, is a constant value.

The governing equations for this problem are the Navier-Stokes equations, the energy equations and the boundary conditions. Boundary conditions are applied at the bubble interface to express (a) the impenetrability (no flow) condition of the normal velocity; (b) the continuity of the tangential velocities; (c) the continuity of normal stress; (d) the continuity of tangential stress, including that due to the thermal variation in surface tension; (e) the continuity of temperature and heat flux; and (f) the finiteness of the variables at the limits of zero and infinity for the radial variable.

The next step in the analysis was to nondimensionalize these expressions, using a minimum parametric representation. The three basic scale factors determined from this method were the stream function, pressure, and velocity given by

$$\Psi_o \quad \frac{a^3}{\mu_1} \frac{d\sigma}{dT} \frac{dT_\infty}{dz} \tag{6}$$

$$P_o = \frac{d\sigma}{dT} \frac{dT_\infty}{dz} \tag{7}$$

$$U_o = \frac{a}{\mu_1} \frac{d\sigma}{dT} \frac{dT_\infty}{dz} \tag{8}$$

Substituting the dimensionless ratios with the scale factors Ψ_o, P_o, U_o, and T_{oo} into the governing equations and boundary conditions, the following dimensionless equations result:

Governing Equations

Stream functions

$$D^4\Psi_1 = -\frac{Ma}{r^2 \sin\theta}\left(\frac{\partial\Psi_1}{\partial\theta}\frac{\partial}{\partial r} - \frac{\partial\Psi_1}{\partial r}\frac{\partial}{\partial\theta} + 2\cot\theta\frac{\partial\Psi_1}{\partial r} - \frac{2}{r}\frac{\partial\Psi_1}{\partial\theta}\right)D^2\Psi_1$$

$$D^4\Psi_2 = -\frac{Ma}{r^2 \sin\theta}\left(\frac{\rho_2}{\rho_1}\frac{\mu_1}{\mu_2}\right)\left(\frac{\partial\Psi_2}{\partial\theta}\frac{\partial}{\partial r} - \frac{\partial\Psi_2}{\partial r}\frac{\partial}{\partial\theta} + 2\cot\theta\frac{\partial\Psi_2}{\partial r} - \frac{2}{r}\frac{\partial\Psi_2}{\partial\theta}\right)D^2\Psi_2 \tag{9}$$

Energy Equations

$$\Pr Ma\left(U - \frac{1}{r^2\sin\theta}\frac{\partial\Psi_1}{\partial\theta}\frac{\partial T_1}{\partial r} + \frac{1}{r^2\sin\theta}\frac{\partial\Psi_1}{\partial r}\frac{\partial T_1}{\partial\theta}\right)$$

$$= \frac{1}{r^2}\frac{\partial}{\partial r}\left(r^2\frac{\partial T_1}{\partial r}\right) + \frac{1}{r^2\sin\theta}\frac{\partial}{\partial\theta}\left(\sin\theta\frac{\partial T_1}{\partial\theta}\right)$$

$$\Pr Ma\left(\frac{K_1}{K_2}\frac{\rho_2}{\rho_1}\frac{C_{p_2}}{C_{p_1}}\right)\left(U - \frac{1}{r^2\sin\theta}\frac{\partial\Psi_2}{\partial\theta}\frac{\partial T_2}{\partial r} + \frac{1}{r^2\sin\theta}\frac{\partial\Psi_2}{\partial r}\frac{\partial T_2}{\partial\theta}\right) \tag{10}$$

$$= \frac{1}{r^2}\frac{\partial}{\partial r}\left(r^2\frac{\partial T_2}{\partial r}\right) + \frac{1}{r^2\sin\theta}\frac{\partial}{\partial\theta}\left(\sin\theta\frac{\partial T_2}{\partial\theta}\right)$$

Boundary Conditions

Normal velocity conditions at the interface

$$\frac{\partial \Psi_1}{\partial \theta} + R' \frac{\partial \Psi_1}{\partial r} = 0$$

$$\frac{\partial \Psi_2}{\partial \theta} + R' \frac{\partial \Psi_2}{\partial r} = 0 \tag{11}$$

Tangential velocity condition at the interface

$$-\frac{R'}{R^2} \frac{\partial \Psi_1}{\partial \theta} + \frac{\partial \Psi_1}{\partial r} = -\frac{R'}{R^2} \frac{\partial \Psi_2}{\partial \theta} + \frac{\partial \Psi_2}{\partial r} \tag{12}$$

Normal stress condition at the interface

$$2\left(\frac{2}{R^3 \sin\theta} \frac{\partial \Psi_1}{\partial \theta} - \frac{1}{R^2 \sin\theta} \frac{\partial^2 \Psi_1}{\partial r \partial \theta}\right) - \frac{2\mu_2}{\mu_1}\left(\frac{2}{R^3 \sin\theta} \frac{\partial \Psi_2}{\partial \theta} - \frac{1}{R^2 \sin\theta} \frac{\partial^2 \Psi_2}{\partial r \partial \theta}\right)$$

$$+ P_2 - P_1 - \left\{\frac{R}{\sin\theta} \frac{\partial}{\partial r}\left(\frac{1}{r^2} \frac{\partial \Psi_1}{\partial r}\right) + \frac{1}{R^3} \frac{\cot\theta}{\sin\theta} \frac{\partial \Psi_1}{\partial \theta} - \frac{1}{R^3 \sin\theta} \frac{\partial^2 \Psi_1}{\partial \theta^2}\right.$$

$$\left. - \frac{\mu_2}{\mu_1}\left[\frac{R}{\sin\theta} \frac{\partial}{\partial r}\left(\frac{1}{r^2} \frac{\partial \Psi_2}{\partial r}\right) + \frac{1}{R^3} \frac{\cot\theta}{\sin\theta} \frac{\partial \Psi_2}{\partial \theta} - \frac{1}{R^3 \sin\theta} \frac{\partial^2 \Psi_2}{\partial \theta^2}\right]\right\} \frac{R'}{R}$$

$$- \frac{\left(\frac{\partial T}{\partial \theta} + \frac{\partial T}{\partial r} R'\right)}{\sqrt{R^2 + R'^2}} \frac{R'}{R} + 2H\left(\frac{\sigma_o}{Ma} - \Delta T\right) = 0 \tag{13}$$

Tangential stress condition at the interface

$$-\left[-2\left(-\frac{1}{R^2}\frac{\cot\theta}{\sin\theta}\frac{\partial\Psi_1}{\partial r}+\frac{1}{R^2\sin\theta}\frac{\partial^2\Psi_1}{\partial r\partial\theta}-\frac{1}{R^3\sin\theta}\frac{\partial\Psi_1}{\partial\theta}\right)\right.$$

$$\left.+2\frac{\mu_2}{\mu_1}\left(-\frac{1}{R^2}\frac{\cot\theta}{\sin\theta}\frac{\partial\Psi_2}{\partial\theta}+\frac{1}{R^2\sin\theta}\frac{\partial^2\Psi_2}{\partial r\partial\theta}-\frac{1}{R^3\sin\theta}\frac{\partial\Psi_2}{\partial\theta}\right)\right]\frac{R'}{R}$$

$$-\frac{R}{\sin\theta}\frac{\partial}{\partial r}\left(\frac{1}{r^2}\frac{\partial\Psi_1}{\partial r}\right)-\frac{1}{R^3}\frac{\cot\partial}{\sin\theta}\frac{\partial\Psi_1}{\partial\theta}+\frac{1}{R^3\sin\theta}\frac{\partial^2\Psi_1}{\partial\theta^2}$$

$$+\frac{\mu_2}{\mu_1}\left[\frac{R}{\sin\theta}\frac{\partial}{\partial r}\left(\frac{1}{r^2}\frac{\partial\Psi_2}{\partial r}\right)+\frac{1}{R^3}\frac{\cot\theta}{\sin\theta}\frac{\partial\Psi_2}{\partial\theta}-\frac{1}{R^3\sin\theta}\frac{\partial^2\Psi_2}{\partial\theta^2}\right]$$

$$+(P_2-P_1)\frac{R'}{R}+\frac{\left(\frac{\partial T}{\partial\theta}+\frac{\partial T}{\partial r}R'\right)}{\sqrt{R^2+R'^2}}+2H\left(\frac{\sigma_o}{Ma}-\Delta T\right)\frac{R'}{R}=0 \qquad (14)$$

where we have used the fact that $\frac{\partial\sigma}{\partial T}=-\left|\frac{\partial\sigma}{\partial T}\right|$.

Temperature continuity at the interface

$$T_1=T_2 \qquad (15)$$

Heat flux continuity at the interface

$$\frac{\partial T_1}{\partial r}-\frac{R'}{R^2}\frac{\partial T_1}{\partial\theta}=\frac{K_2}{K_1}\left(\frac{\partial T_2}{\partial r}-\frac{R'}{R}\frac{\partial T_2}{\partial\theta}\right) \qquad (16)$$

Condition at finiteness as radius approaches zero

$$\Psi_2 \rightarrow \text{finite} \tag{17}$$

Condition at uniform flow as radius approaches infinity

$$\Psi_1 = \frac{1}{2} U r^2 \sin^2 \theta \tag{18}$$

Boundedness conditions on temperatures

$$T_1, T_2 \rightarrow \text{finite as } |r| \rightarrow \infty, o \tag{19}$$

The dimensionless groupings appearing in the above equations are:

$$\text{Ma, Pr, } \frac{\rho_2}{\rho_1}, \frac{\mu_2}{\mu_1}, \frac{K_2}{K_1}, \frac{C_{p_2}}{C_{p_1}}, \sigma_o$$

They are defined as:

$\text{Ma} = \dfrac{\rho_1 a^2}{\mu_1^2} \left|\dfrac{d\sigma}{dT}\right| \dfrac{dT_\infty}{dz}$ which is called the Marangoni number, Pr is the Prandtl number, $\dfrac{\rho_2}{\rho_1}, \dfrac{\mu_2}{\mu_1}, \dfrac{K_2}{K_1}, \dfrac{C_{p_2}}{C_{p_1}}$ are the dimensionless ratios of density, viscosity, thermal conductivity and specific heat, and, finally,

$$\sigma_o = \frac{\bar{\sigma}_o \rho_1 a}{\mu_1^2}$$

All of the above dimensionless groupings are calculable, based on known fluid thermophysical properties, a temperature gradient, and a characteristic length. It is noteworthy to mention that once the fluids are chosen, there are only two control parameters remaining, namely the temperature gradient, dT_∞/dz, and the characteristic length, usually the bubble radius, both of which appear as part of the Marangoni number. The general equations governing the motion of a

deformable bubble, including the boundary conditions in a nonisothermal liquid, have now been derived in dimensionless form. The next step in the analysis is to obtain analytical solutions.

Parameter Perturbation Theory

Parameter perturbation theory was used to solve the governing equations together with the appropriate boundary conditions. In this theory we seek a solution to the boundary value problem in terms of a control parameter, that is, the dependent variables are expanded in terms of this control parameter. Basically, what is done to determine approximate solutions to differential equations, whether they be governing equations or boundary conditions, is to assume expansions, substitute them into the equations, and then solve the equations. An important class of such asymptotic sequences is represented as a collection of integer powers of the perturbation parameter, in this case, the Marangoni number. The general expression for a variable $f(\bar{r}, Ma)$ is given by

$$f(\bar{r}, Ma) = \sum_{n=0}^{\infty} a_n(\bar{r}) Ma^n \tag{20}$$

as the Ma approaches zero, where $a_n(\bar{r})$ is an expansion variable. This is a straightforward expansion of the Poincare' type and is used in this analysis. Care must be taken to insure that the expansion is uniformly valid. As a result of making these substitutions, sets of equations for the zeroth-, first-, and second-order equations for both the governing equations and the boundary conditions are obtained. Solutions for these sets of equations are obtained. Young, et al. (ref. 3) obtained the zeroth-order solution, and Bratukhin (ref. 9) presented the first-order approximation. Second-order solutions were obtained in reference 10 for the stream functions, temperature, and pressure distributions in the inner and outer media, and expressions for the bubble terminal velocity and the bubble deformation. In dimensionless form, the bubble deformation and

the terminal velocity (in terms of Reynolds number) are

$$R = 1 - \frac{1}{\sigma_o}\left(\frac{15}{128} + \frac{7}{144}\,\mathrm{Pr}\right)\left(\frac{3\cos^2\theta - 1}{2}\right)\mathrm{Ma}^2$$

$$- \frac{1}{\sigma_o}\left[\frac{207}{260}\,\frac{1}{\sigma_o}\left(\frac{15}{128} + \frac{7}{144}\,\mathrm{Pr}\right) - \frac{9}{13,312} + \frac{9\,\mathrm{Pr}}{53,248} - \frac{\mathrm{Pr}^2}{1,248}\right]$$

$$\times \left(\frac{5\cos^3\theta - 3\cos\theta}{2}\right)\mathrm{Ma}^3 \qquad (21)$$

and

$$\mathrm{Re} = \frac{\mathrm{Ma}}{2} + \left[\frac{1}{\sigma_o}\left(\frac{15}{128} + \frac{7}{144}\,\mathrm{Pr}\right) - \frac{9}{1,280} + \frac{3}{320}\,\mathrm{Pr} - \frac{147}{8,640}\,\mathrm{Pr}^2\right]\mathrm{Ma}^3 \qquad (22)$$

In this case the bubble radius is a function of the Prandtl number and the dimensionless parameter σ_o for both the first- and second-order approximations. On the other hand, the terminal velocity is affected by the zeroth- and the second-order approximations, that is, there is no contribution to the terminal velocity resulting from the first-order approximation. Here too, the second-order effect is a function of the Prandtl number and the parameter σ_o.

Surface tension variation must be included in this analysis. It is important to note that the Navier-Stokes equations and the energy equations are thereby coupled through the normal and shear stress boundary conditions which contain surface tension terms, and the surface tension is a function of the liquid temperature.

It was shown from the analysis that no nonuniformities result from the substitution of lower-order solutions into the governing equations and boundary conditions to obtain higher-order solutions. Thus, the dependent variables can be

expanded in a straightforward manner in terms of integer powers of the Marangoni number. Generally, the nonuniformity condition which arises in isothermal bubble motion in normal gravity results because the uniform velocity condition as $|r|$ approaches infinity cannot be satisfied in the first approximation. This is commonly referred to as Whitehead's paradox. In the present study, this did not occur in the first- and second-order approximations. However, based on the results of the second-order approximation, it is suggested by the author (ref. 10) that higher-order approximations, third and fourth order, may result in the development of a nonuniformity condition, that is, the boundary condition of uniform velocity at infinity will not be satisfied. This conclusion is based on the presence of the Skokeslet term, which is the r term, in the second-order approximation of the stream function. This condition on the straightforward expansion may not appear until the fourth-order approximation, which should contain the next approximation to the bubble terminal velocity. At some higher order, the boundary condition at infinity cannot be satisfied. At that point another solution technique would have to be used, such as a matched asymptotic expansion, integral, or numerical method.

COMPARISON OF EXPERIMENTAL AND THEORETICAL RESULTS

Experimental and theoretical results for ethylene glycol and silicone oil are plotted in Figure 9. For the experimental data, the Marangoni number is plotted against the Reynolds number for single bubbles. Theoretical results are plotted for both the zeroth-order and the higher-order solutions. The zeroth-order solution (creeping flow), given by the first term in equation (22), is shown as the solid line. As was determined earlier, the higher-order solution, which includes the second-order approximation given by the second term in equation (22), has a very limited range of applicability, even for the limiting case where the Prandtl number approaches zero and the dimensionless

parameter σ_o approaches infinity. The dashed line (theoretical result) shown in Figure 9 illustrates this case graphically; it deviates from the experimental results very sharply for Reynolds numbers greater than 1.5. What is, however, most noteworthy from this figure in comparing experimental and theoretical results, is that the experimental data generally match the zeroth-order solution, even for the relatively high Marangoni numbers. In other words, for Marangoni numbers greater than 0.1, the theory is not expected to be applicable, but it apparently is. From the first-order approximation, it is predicted that, independent of the Prandtl number, a standing eddy should begin to form behind a bubble when the Marangoni number is approximately equal to 16/3. As the standing eddy begins to develop, it should result in changing the surface tension gradient over the rearward portion of the bubble interface. If this occurs, the experimental results should begin to deviate from the theoretical results at Marangoni numbers greater than 16/3. Comparing this analytical result with the experimental data in Figure 9, the data show that there is very little deviation from the zeroth-order solution up to Marangoni numbers of about eight. Substitution of typical values for Prandtl number and σ_o for these test liquids into the expression for first- and second-order bubble deformation predicts that the bubble should change shape for intermediate values of Marangoni numbers. However, in every test, the bubble shape, after the initial oscillations damped out, remained spherical. This suggests that the equation for bubble deformation is valid for liquids having Prandtl numbers on the order of one. The number of data points is rather limited and before any definitive conclusions can be drawn from the comparison of the experimental and theoretical results, additional data points are needed. In particular, if comparisons are to be made at very low Marangoni numbers using relatively high viscosity test liquids, much longer zero-gravity times than the 5.2 seconds obtained in the drop tower are required. In fact, it would also be

desirable to have longer zero-gravity times over which to take data for the higher Marangoni numbers.

A compilation of all of the experimental data, including the multiple-bubble as well as the single-bubble data, is presented in Figure 10 for the three test liquids in which Marangoni flow was observed. Data points for multiple bubbles are included on this figure since arguments were made earlier to validate their usefulness. For the multiple-bubble data points, the subscripts L and T are used, where the subscript L indicates a leading bubble and the subscript T indicates a trailing bubble. For comparison, the zeroth-order approximation is shown as the solid line in the figure. The dashed line through the data points indicates that at the higher Marangoni numbers, the experimental data does deviate from the theory. One possible explanation for the deviation is that perhaps a standing eddy is being formed behind the bubble, as predicted from the first-order solution mentioned previously. As the standing eddy grows, the surface tension gradient is affected more and more, thus causing the bubble terminal velocity to decrease, which correspondingly reduces the Reynolds number. As was determined earlier, the bubble shape does not affect the bubble terminal velocity. The bubble remains spherical, in contradiction to the theory. The data shown in this figure prove the existence of the Marangoni flow phenomenon, and should serve as a basis for a continuing research effort in this area, both experimentally and analytically.

CONCLUSIONS AND RECOMMENDATIONS

The principle conclusion of this research is that the Marangoni bubble motion flow phenomenon does occur and can be a driving flow mechanism in a zero-gravity environment. For the first time, it has been shown experimentally that local surface tension variations at the bubble interface caused by a temperature gradient in the liquid cause the bubble to migrate from the cold to the hot region and thus the flow phenomenon is real. This flow phenomenon was ob-

served in three out of the four test liquids used. The range of Reynolds numbers was from about 0.25 to 90, with corresponding Marangoni numbers ranging from about 0.50 to 600. This flow phenomenon was not observed in distilled water.

Comparison of the experimental with the theoretical results were made on the basis of bubble terminal velocity. Experimental data could be correlated in terms of two parameters, namely the Reynolds number and the Marangoni number. In the zeroth-order approximately solution, the Reynolds number was proportional to the Marangoni number, and it was proved analytically that the bubble must remain spherical. Although the theory in this case would be expected to be valid only for Marangoni numbers much less than one, the theory was in good agreement with experimental data for Marangoni numbers up to about eight, at which point the data begins to deviate from theory. Experimental data also corroborated the analytical result that the bubble remains spherical. Not only was this the case for small Marangoni numbers, but for Marangoni numbers approaching 600 as well, which contradicts higher-order theory.

A dimensional analysis was performed on the governing equations which include the Navier-Stokes equations and the energy equations together with the appropriate boundary conditions for the inner and outer media. The following dimensionless ratios and groupings evolved: viscosity, density, thermal conductivity, and specific heat ratios of the inner and outer media, and the dimensionless parameters, the Marangoni number and the Prandtl number, expressed in terms of the outer medium fluid properties. Two other dimensionless groupings are the uniform velocity of the liquid at infinity and a grouping expressed as

$\sigma_o = \frac{\bar{\sigma}_o \rho_1 a}{\mu_1^2}$. Once the inner and outer media are chosen, there are only two control parameters remaining, namely, the temperature gradient and the characteristic length, which in this case is the bubble radius. Both of these parameters appear in the Marangoni number. For this reason, it was concluded that the control parameter that should be used in parameter perturbation theory was the Marangoni number. In other words, all the dependent variables are expanded in terms of the Marangoni number.

In the first-order approximation, the bubble deformation depended not only on the Marangoni number, but also on the Prandtl number and the dimensionless parameter σ_o. Bubble deformation, however, was not experimentally observed, and this disagreement is due to the theory only being valid for the limiting case of Prandtl numbers less than one and values of the dimensionless parameter σ_o approaching infinity. The bubble terminal velocity was the same as in the zeroth-order approximation.

From the first-order approximation, independent of the Prandtl number, it was also found that a standing eddy should begin to form behind a bubble when the Marangoni number is approximately equal to 16/3. As the eddy develops, it should result in changing the surface tension gradient over the rearward portion of the bubble. If the eddy does occur, the experimental data should begin to deviate from the theoretical results at a Marangoni number somewhat greater than 16/3. The data indeed begins to deviate from theory in the Marangoni range of 6 to 10, which is consistent with theory.

From the second-order approximate solution, it was determined that there was a second-order effect on both the bubble shape and its terminal velocity. The solutions for predicting second-order effects on bubble shape and bubble terminal velocity are valid if the Prandtl number is on the order of one and

the dimensionles parameter σ_o is large. Unfortunately the data obtained were for liquids having Prandtl numbers much greater than one, and, therefore, the theory cannot be directly compared with the data. It is, however, worth mentioning that one area where the second-order approximations for bubble terminal velocity, or Reynolds number, and bubble deformation may have some application is for liquid metals. In the case of liquid metals, the Prandtl numbers are much less than one. Marangoni bubble motion experiments would have to be performed in a space environment, such as in Spacelab, where long zero-gravity times are available.

The experimental data obtained in the present study prove the existence of the Marangoni flow phenomenon for bubble motion, and should serve as a basis for a continuing research. The following are areas where continuing research efforts could profitably be directed:

1. It would be desirable to obtain data points for several test liquids in order to evaluate the effect of Prandtl number and the dimensionless parameter, σ_o, on the bubble terminal velocity and shape, as suggested from higher-order approximate solutions. Although the experiment does not agree with the higher-order approximations, qualitatively, the bubble terminal velocity and bubble shape may depend on a functional relationship of these two dimensionless parameters. In other words, different curves of Reynolds number versus Marangoni number may be obtained as σ_o and Prandtl number are varied.

2. It would also be desirable to obtain data for a given Marangoni number by varying the two control variables, namely, the temperature gradient and the bubble radius, to see if the bubble terminal velocity, or correspondingly, the Reynolds number is affected. For example, as the bubble radius is decreased below 1 centimeter, the temperature gradient must be increased in proportion to the radius squared in order to keep the Marangoni number a constant. Of course, this means that much higher temperature gradients would be required

than those obtained as part of this experiment, and this would require much longer heating times.

3. Additional data should be obtained at very low Marangoni numbers (the creeping flow regime), so that theory can be compared with experimental data. This could be accomplished by using relatively low viscosity fluids, such as silicone oil, and would require much longer zero-gravity times than the 5.2 seconds obtained in the drop tower. It would also be desirable to have longer zero-gravity times at the higher Marangoni numbers because of uncertainties about whether the bubble formation and separation processes disturb the temperature field.

4. Data should be obtained for bubble expansion resulting from heating by the liquid. Much longer zero-gravity times than those obtained in the drop tower are required. In all the nonisothermal experiments conducted in the drop tower, there was no discernible change in bubble size.

5. To extend the perturbation analysis to higher-order approximations does not appear to be profitable at this time until low Prandtl number data are obtained. Perhaps better higher-order approximations could be achieved using parameter perturbation theory to match the intermediate Marangoni number experimental data by expanding the dependent variables about a control or expansion parameter other than the Marangoni number, for example, the Prandtl number times the Marangoni number.

6. Another logical step in extending the analysis is to solve the governing equations, together with the boundary conditions presented in this paper, numerically. If this is achieved, the final step would be to allow the thermophysical properties to be temperature dependent.

SYMBOLS

a	spherical bubble radius
$a_n(r, \theta)$	expansion variable
C_p	specific heat
D	scalar differential operator
f	function
g	gravitational acceleration
H	mean radius of curvature
h	thermal conductivity
K	thermal conductivity
Ma	Marangoni number
n	integer
Pr	Prandtl number
R	deformed bubble radius
Re	Reynolds number
r	radius in spherical coordinates
T	temperature
dT_∞/dz	temperature gradient at infinity
U	bubble terminal velocity
z	polar axis
θ	polar angle in spherical coordinates
μ	viscosity

ρ	density
$\bar{\sigma}_o$	reference surface tension
σ_o	dimensionless group
$d\sigma/dT$	surface tension gradient
Ψ	stream function

Subscripts:

1, 2	outer and inner media
o	scale factor

Superscript:

$( )'$	derivative

REFERENCES

1. Hershey, A. V., "Ridges in a Liquid Surface Due to the Temperature Dependence of Surface Tension," Phys. Rev., 56, 204 (1939).
2. Block, M. J., "Surface Tension as the Cause of Benard Cells and Surface Deformation in a Liquid Film," Nature, 178, 650 (1956).
3. Young, N. O., J. S. Goldstein, and M. J. Block, "The Motion of Bubbles in a Vertical Temperature Gradient," J. Fluid Mech., 6, 350 (1959).
4. Hardy, S. C., " The Motion of Bubbles in a Vertical Temperature Gradient," J. Colloid Interface Sci., 69, 157 (1979).
5. McGrew, J. L., "An Investigation of the Effect of Temperature Induced Surface Tension Gradients on Bubble Mechanics and Boiling Heat Transfer," Ph.D. thesis, University of Denver, Denver, (1968).
6. Papazian, J. M. and W. R. Wilcox, "Flight 1 Technical Report for Experiment 74-36-Thermal Migration of Bubbles and Their Interaction with Solidification Interfaces," NASA CR-144304 (1976).
7. Kuznetsov, V. M., B. A. Lugovtsov, and E. I. Sher, "Motion of a Gas Bubble in a Liquid Under the Effect of a Temperature Gradient," Zh. Prikl. Mekh. Tekh. Fiz., p. 124 (Jan.-Feb. 1966).
8. Lyubin, L. Ya and A. S. Povitskiy, "Thermal Capillarity in a Liquid in the Absence of Body Forces," Zh. Prikl. Mekl. Tekh. Fiz., No. 2, 40 (1961).
9. Bratukhin, Yu. K., "Thermocapillary Drift of a Viscous Fluid Droplet," Izv. Akad. Nauk SSSR. Mekh. Zhidk. Gaza, No. 5, 156 (1975). Also NASA TT F-17093 (1976).
10. Thompson, R. L., "Marangoni Bubble Motion in Zero Gravity," Ph.D. thesis, The University of Toledo, Toledo, (1979).

TABLE 1. - THERMOPHYSICAL PROPERTIES OF FLUIDS AND GAS

(Properties are valid between 20° and 25° C)

	Distilled water	Ethylene glycol	Ethanol	Silicone oil DC-200	Nitrogen
Density, gm/cc	1.0	1.11	0.78	0.94	0.00125
Viscosity, poise	0.009	0.138	0.011	0.103	0.000178
Thermal conductivity, cal/sec cm °C	0.00143	0.000627	0.00040	0.00032	0.000056
Surface tension, dynes/cm	73.0	46.9	22.3	20.1	--------
Surface tension temperature coefficient, dynes/cm °C	-0.16	-0.077	-0.084	-0.07	--------
Prandtl number	7	126	15	137	0.8

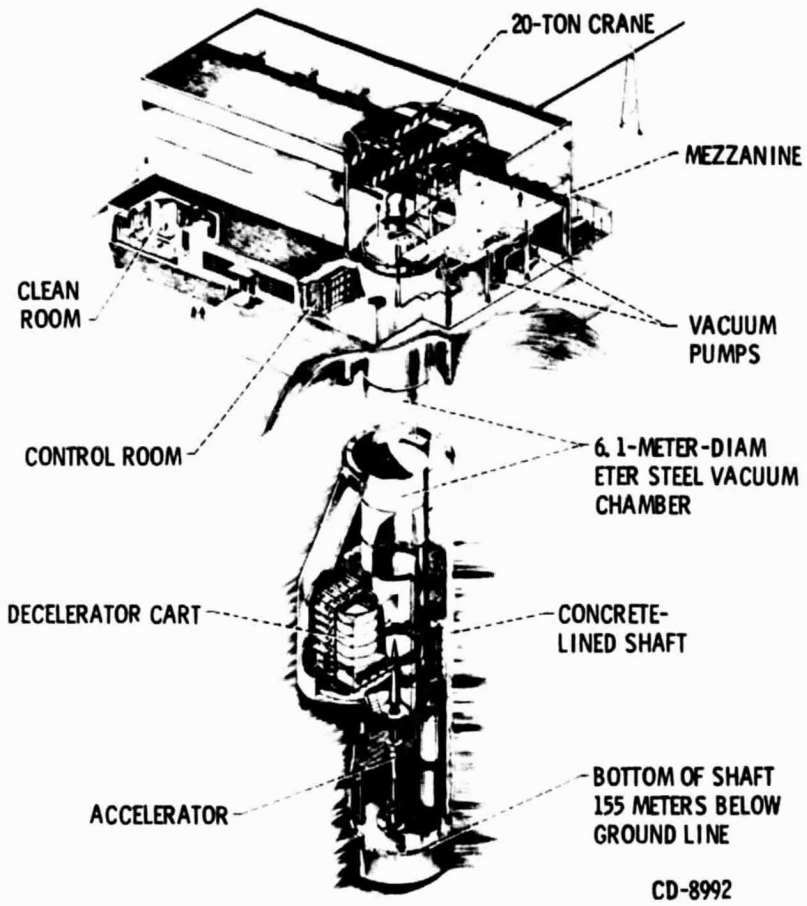

Figure 1. - NASA zero-gravity facility.

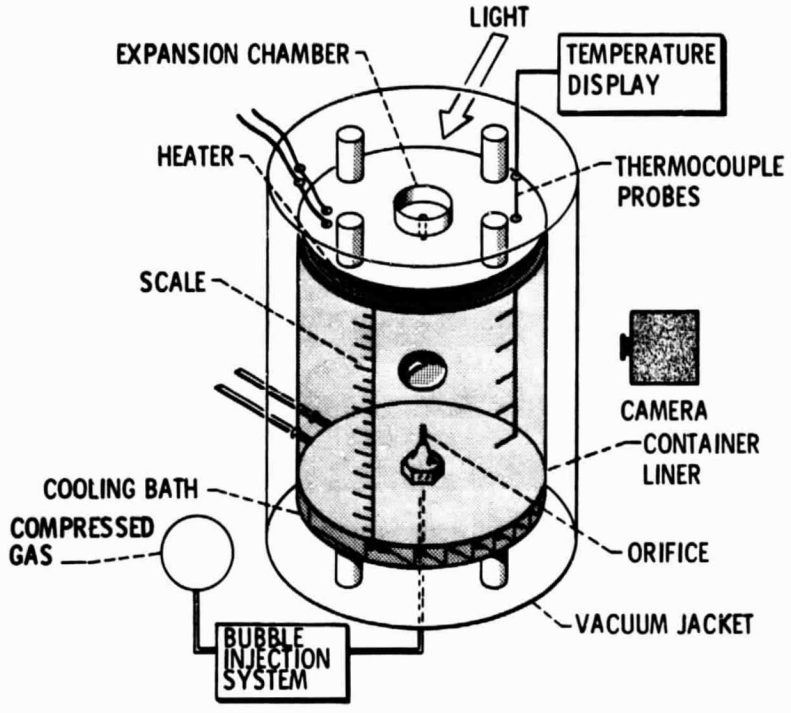

Figure 2. - Schematic of experimental apparatus.

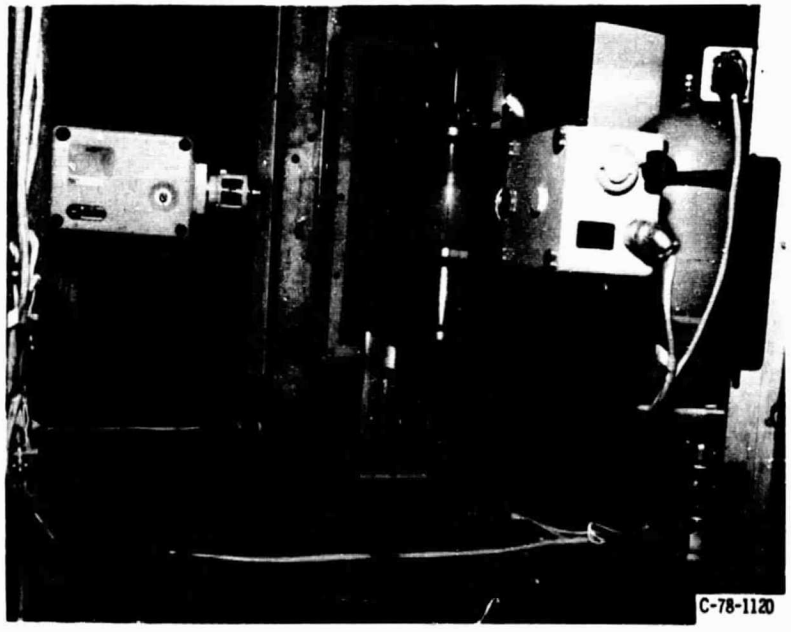

Figure 3. - Zero-gravity experimental apparatus.

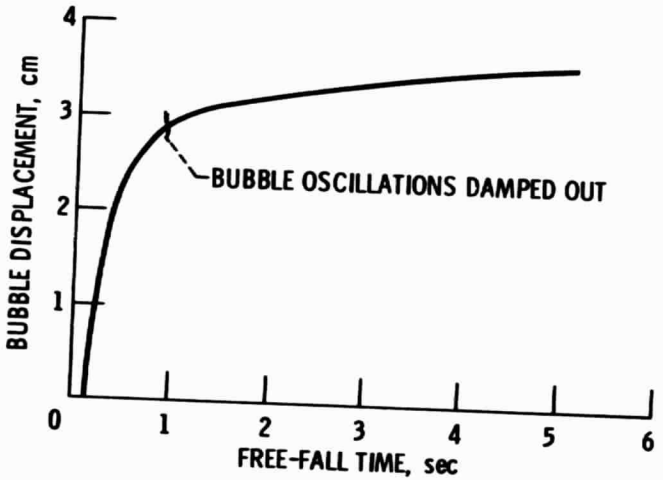

Figure 4. - Bubble displacement in an isothermal liquid (distilled water).

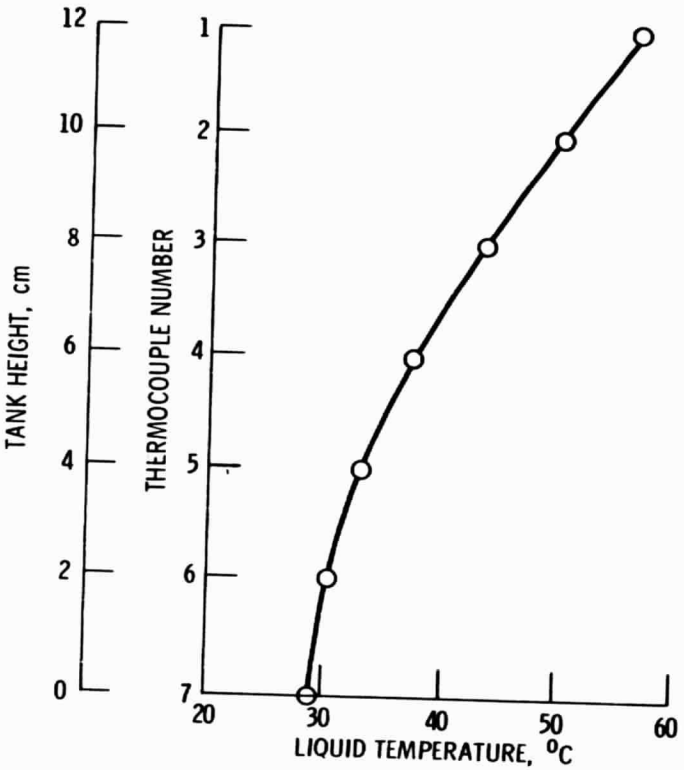

Figure 5. - Typical final liquid temperature profile for distilled water after 260 minutes of heating.

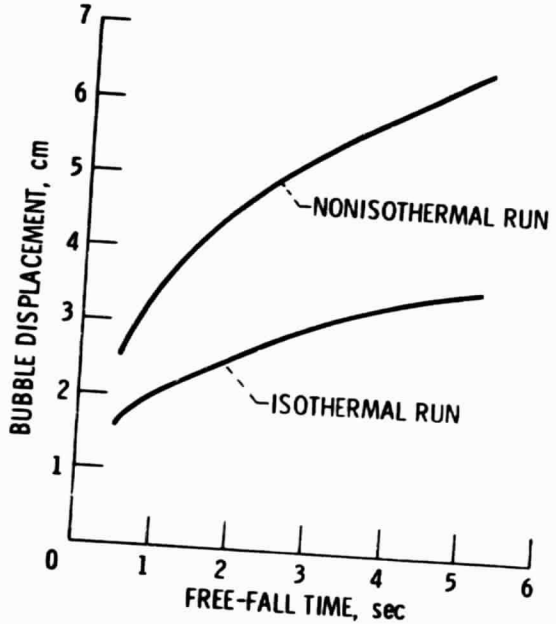

Figure 6. - Comparison of nonisothermal and isothermal bubble displacement (distilled water).

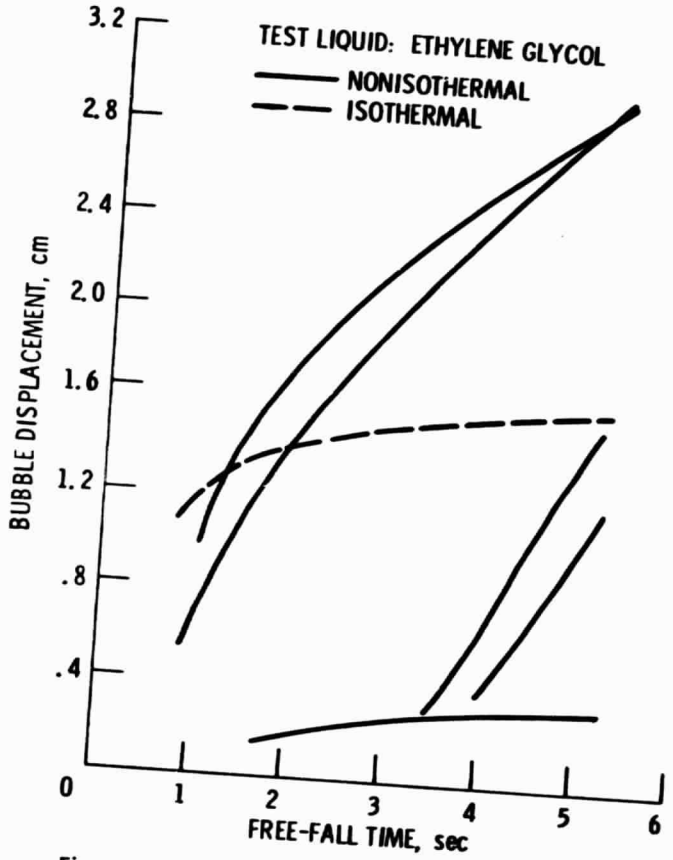

Figure 7. - Comparison of nonisothermal and isothermal bubble displacement.

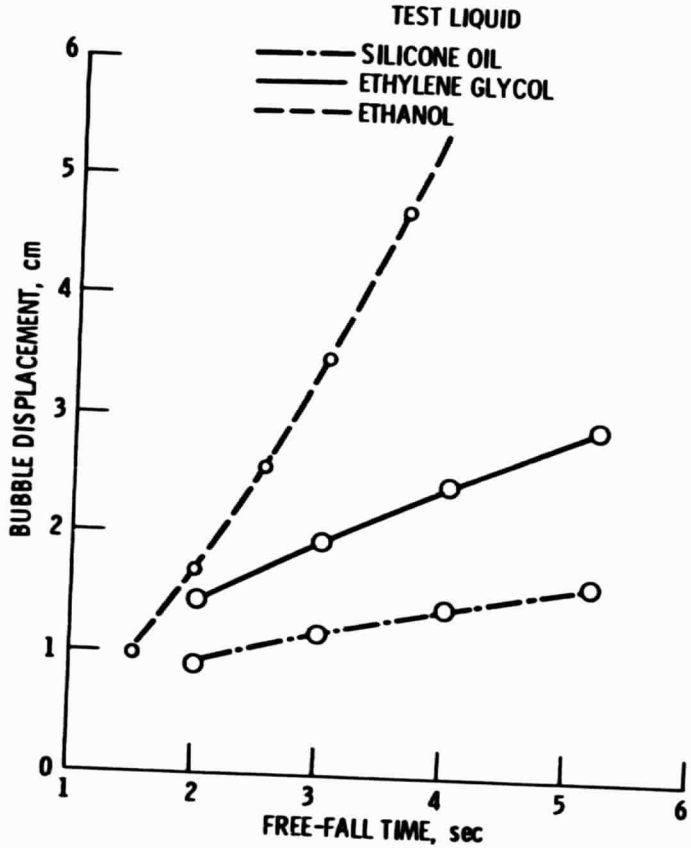

Figure 8. - Typical bubble displacements for nonisothermal liquids.

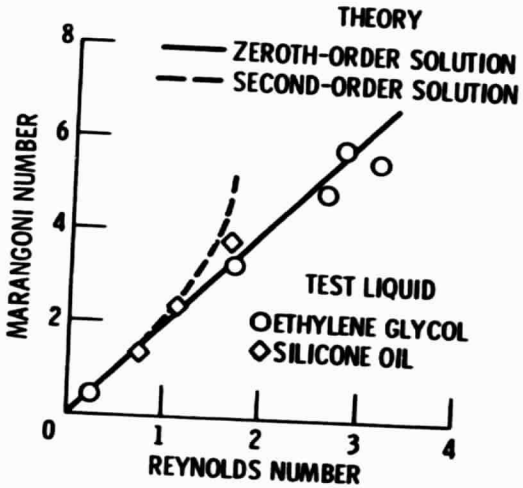

Figure 9. - Comparison of experimental versus theoretical results for a single bubble.

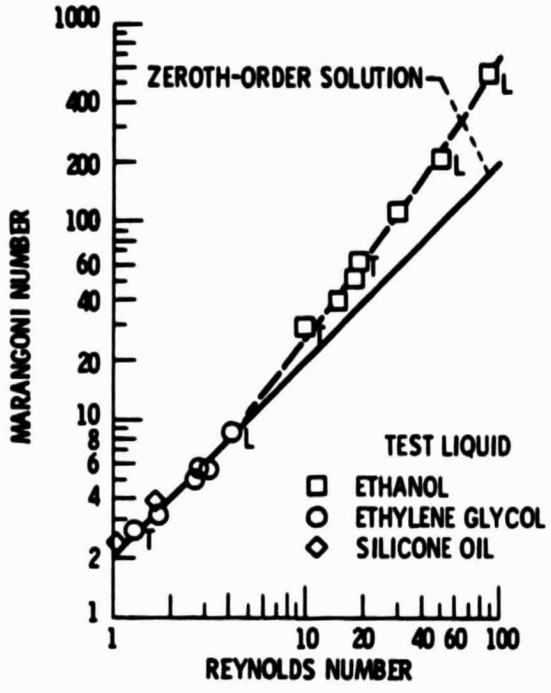

Figure 10. - Summary of experimental versus theoretical results for single and multiple bubbles.